

pubs.acs.org/NanoLett Letter

# Net Unidirectional Fluid Transport in Locally Heated Nanochannel by Thermo-osmosis

Xin Wang, Maochang Liu, Dengwei Jing, Abdulmajeed Mohamad, and Oleg Prezhdo\*



Cite This: Nano Lett. 2020, 20, 8965-8971



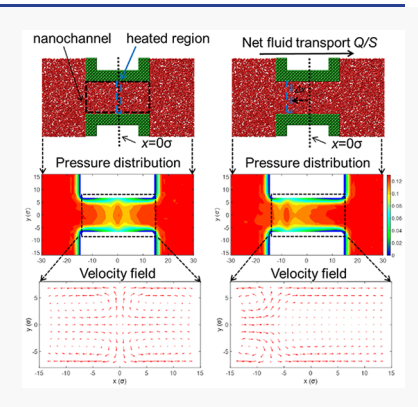
**ACCESS** 

Metrics & More

Article Recommendations

Supporting Information

ABSTRACT: Thermo-osmosis driven by temperature gradients generally requires two liquid reservoirs at different temperatures connected by porous bodies or capillaries. We demonstrate, by molecular dynamics simulation, a new phenomenon toward nanoscale thermo-osmosis. Upon heating at a certain region of a nanochannel, multiple nanoscale convective layers are formed and can be manipulated to generate a net fluid transport from one reservoir to another, even without a temperature difference between them. A net unidirectional fluid transport with different rates can be achieved by precisely controlling location of the heated region. The net fluid transport can be enhanced further by tuning liquid-wall interactions. The demonstrated phenomenon provides a strategy for enhancing fluid mixing, which is often inefficient in nanoscale flows. Our finding is promising for chiplevel cooling. The heat generated by chips can be employed to produce asymmetric temperature gradients in channels through proper configuration. Coolant liquids can thus be circulated without extra pumps.



KEYWORDS: thermo-osmosis, interfacial flow, nanofluidics, molecular dynamics

anofluidics is the study of fluids and ionic species transport at nanometer scale. Considerable progress reported in past years render this emerging field charming and blooming.<sup>2-11</sup> On a macroscopic scale, fluid is driven by pressure gradients or body forces, such as gravity and centrifugal forces. In nanofluidics, however, fluid flow is dominated by surface effects, where transport is caused by electric fields, concentration gradients, and temperature gradients near the interfaces, that is, electro-osmosis, diffusioosmosis, and thermo-osmosis, respectively. It becomes more important to understand and predict these osmotic flows from molecular level with the development of nanofluidics. Compared with electro-osmosis, 12-13 very limited work has been done on thermo-osmosis so far. Thermo-osmosis was observed and reported by Lippmann in 1907. 16 The applications of thermo-osmosis range from biological to energy areas, such as optothermal DNA trapping and identification of protein aggregates, <sup>17,18</sup> wastewater recovery, <sup>19,20</sup> energy harvesting from temperature gradients, <sup>21,22</sup> fuel cells, <sup>23,24</sup> and so on.25

In the last century, thermo-osmosis was studied mainly in the experimental system, where two liquid reservoirs with a temperature difference were separated by a porous membrane. The porous membranes were black boxes. Limited by previous experiment technology, it was difficult to observe what happened inside the membrane. Recently, Bregulla et al. reported the first microscale observation of thermo-osmotic flow by tracking single tracer nanoparticles in the microchannel, providing direct evidence of thermo-osmosis. 27

However, it is still a challenge to measure the local velocity, enthalpy, pressure, and viscosity on the nanometer scale.

In this regard, molecular dynamics (MD) simulations play a critical role in the mechanistic study of thermo-osmosis flow. In fact, directly simulating thermo-osmosis is very difficult because no corresponding explicit force is reasonably available to act on the simulated particles. Nevertheless, some progress has been made recently. Ganti et al. employed equilibrium MD simulation to study the local pressure difference distribution near the solid—liquid interface under different temperatures. The result suggested that it should be feasible to consider thermo-osmosis without any external assumption using MD simulation. Fu et al. further used nonequilibrium MD simulation to study a practical case. The influence of stagnant layer, slip length, and viscous entrance was studied. This work provided a more detailed molecular-level understanding of thermo-osmosis.

On the other hand, new phenomena are expected to emerge by breaking the homogeneities or symmetries of surfaces in nanofluidics. For instance, a net electro-osmotic flow was achieved by breaking geometric symmetries.<sup>30</sup> A fluid was pumped by symmetric temperature gradients with heteroge-

Received: October 29, 2020 Revised: November 14, 2020 Published: November 24, 2020





neous surface energies.<sup>31</sup> Rectified flows were realized on composite surfaces with inhomogeneous surface charges,<sup>32</sup> surface energies,<sup>33</sup> and shapes of nanochannels.<sup>34</sup>

Inspired by these works, we propose a new approach employing the power of thermo-osmosis where a certain region inside the nanochannel is heated, while both of the reservoirs at the ends of nanochannel are kept at the same temperature. This situation can be realized experimentally by laser illumination of sufficiently long nanochannels, longer than the simulation system that is limited by computational cost. For instance, Bregulla et al. used a laser to heat a gold nanoparticle which was fixed on the wall surface.<sup>27</sup> The local heating induced a temperature gradient and a thermo-osmosis flow was driven. This local heating technique finds various applications, such as photothermal cancer therapy and manipulation of micron-sized objects and nanoparticles.<sup>35</sup> Especially, we explore what would happen when the symmetrical temperature gradients are broken, which is achieved by controlling the location of the heated region. Are there any new phenomena or properties? The answer is definitely positive. Molecular dynamics simulation reveals two significant phenomena, including the formation of steady multiple convective layers in the nanochannel, and a net fluid transport from one reservoir to another even without temperature difference between the reservoirs. The physical mechanisms that govern these phenomena are investigated. We focus on the role of slip length on the amplification of the velocity field. The influence of liquid-wall interaction, the height of the channel, and heating on the directions and rates of fluid transport are also considered. Finally, we demonstrate several possible applications for the observed phenomena.

Here, we present briefly the simulation setup. The details can be found in the <u>Supporting Information</u>. All the simulations have been performed with the LAMMPS package.<sup>36</sup> The interaction among the particles are described by Lennard-Jones (LJ) potentials

$$V(r) = 4\varepsilon \left[ \left( \frac{\sigma}{r} \right)^{12} - \left( \frac{\sigma}{r} \right)^{6} \right]$$
 (1)

where r is the distance between particles, and  $\varepsilon$  and  $\sigma$  are energy and length parameters, respectively. A spring force is applied to each solid particle to tether it to its initial position to prevent melting. To construct the system, a nanochannel is connected by two liquid reservoirs, Figure 1. The system is first

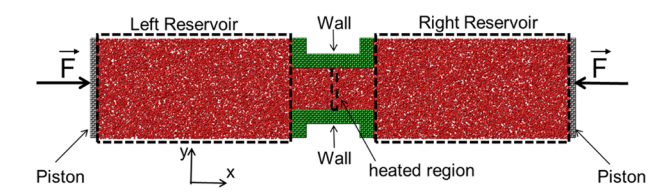
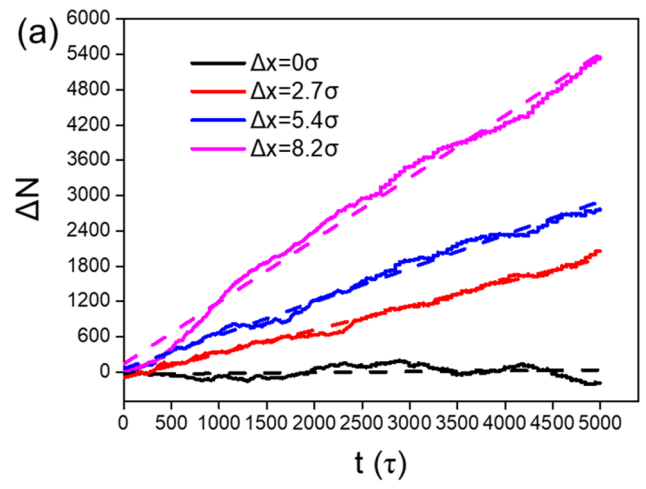


Figure 1. Snapshot of the system used in MD simulations.

run under the NVT ensemble at  $T=0.85\varepsilon/k_{\rm b}$ . Then the temperature in the heated region is increased to achieve a local heating. The Nose-Hoover thermostat is used. The liquid between the heated region and the reservoirs, and the walls are run under the NVE ensemble. We have confirmed that the choice of different thermostatting methods has little influence on the results. The details can be found in the Supporting Information.

Before the simulation, the effect of liquid-wall energy on wetting behavior is evaluated to determine the rough range of  $\varepsilon_{\text{liquid-wall}}$  in order to cover both hydrophobic and hydrophilic conditions. As shown in Figure S1, a liquid droplet, including 4000 particles, is laid on a solid surface at  $T=0.85\varepsilon/k_{\text{b}}$ . The simulation details can be found in the Supporting Information. The formed contact angles  $\theta$  vary with  $\varepsilon_{\text{liquid-wall}}$ , as shown in Figure S2.

A hydrophobic nanochannel is considered first by adopting  $\varepsilon_{\rm liquid\text{-}wall}$  as  $0.3\varepsilon$  ( $\theta\sim115^\circ$ ). The fluid transport is studied by changing the locations of the heated region in the nanochannel. The number variations of liquid particles in the right reservoir  $\Delta N$  are recorded, as shown in Figure 2a. The average



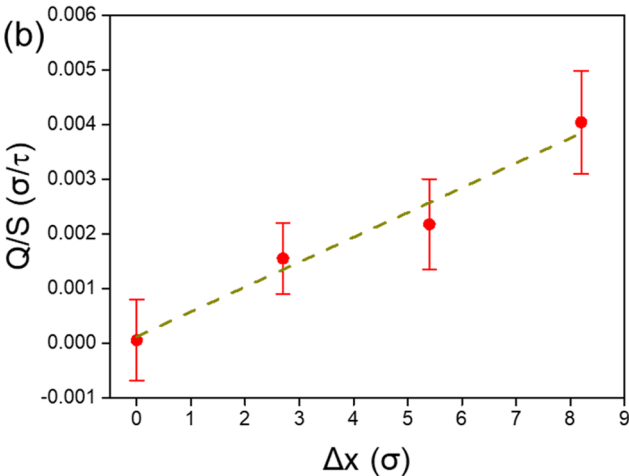


**Figure 2.** (a) Number variations of liquid particles in right reservoir  $\Delta N$  as a function of time. Solid lines represent the MD results and dashed lines represent the linear fit used to compute the rates of net fluids transport Q/S according to eq 2. (b) Rates of net fluids transport Q/S as a function of locations of heated region. Here,  $\Delta x$  means the distance that heated region is shifted from the center to the left. Error bars represent the standard deviation of eight independent simulations.

rate of net fluid transport  $v_a$  can be deduced form the linear fit of the time-dependent variation of the number of the particles

$$v_{\rm a} = \frac{Q}{S} = \frac{\Delta N}{S\rho \Delta t} \tag{2}$$

where Q is the volume flow rate, S is the cross-section area of the nanochannel, and  $\rho$  is the liquid density. The predicted

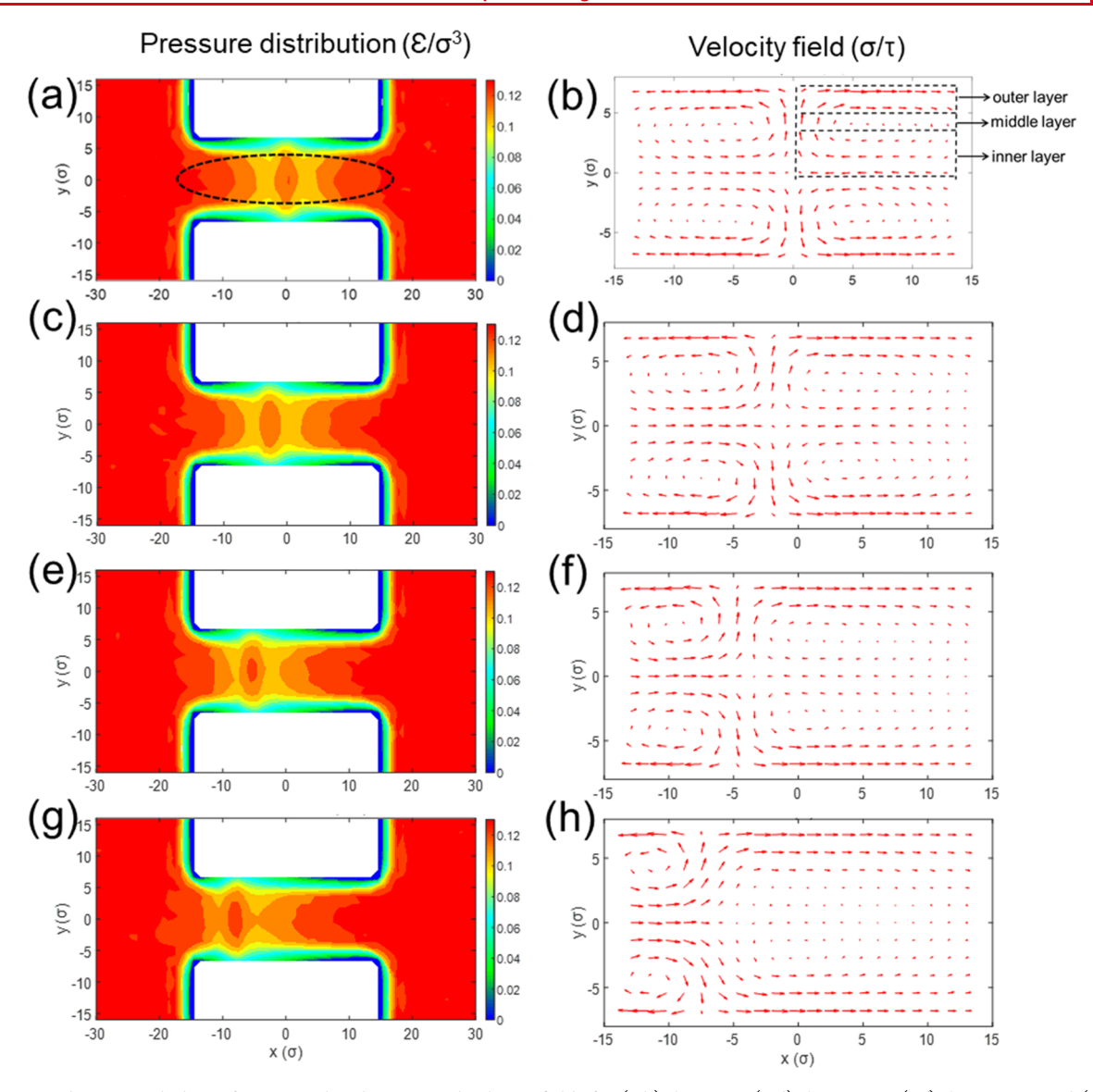


Figure 3. Two-dimensional plots of pressure distributions and velocity fields for (a,b)  $\Delta x = 0\sigma$ , (c,d)  $\Delta x = 2.7\sigma$ , (e,f)  $\Delta x = 5.4\sigma$ , and (g,h)  $\Delta x = 8.2\sigma$ , when  $\varepsilon_{\text{liquid-wall}} = 0.3\varepsilon$ ,  $\Delta t = 0.4\varepsilon/k_b$ , and  $h = 14.96\sigma$ .

results are shown in Figure 2b. When the heated region is located in the center of the nanochannel, that is,  $\Delta x = 0\sigma$ , fluid transport is hardly observed. When the heated region moves leftwards for a certain distance, that is,  $\Delta x = 2.7\sigma$ ,  $5.4\sigma$ , and  $8.2\sigma$ , a continuous net fluid transport from the left reservoir to the right emerges and increases with increases of  $\Delta x$ .

To reveal the physical mechanism of the flow, the velocity field in the nanochannel for the case of  $\Delta x = 0\sigma$  is investigated, as shown in Figure 3b. The velocity field can be divided into multiple convective layers: the outer layers (near the wall surfaces), the middle layer, and the inner layer (far from the wall surfaces). Because the velocity field is symmetrical, only a quarter part is marked. In the outer layers, the velocity is controlled by thermo-osmosis. The velocity asymptotically decreases to zero in the middle layer. The velocity field direction inverts in the inner layer. The formed convective layers are assumed to depend on the extent of thermo-osmosis. Derjaguin related the thermo-osmotic velocity  $\nu_{\rm t}$  to the interfacial excess enthalpy based on Onsager reciprocal relations using linear nonequilibrium thermodynamics<sup>37</sup>

$$v_t = \beta_{12} \frac{\nabla T}{T} = -\frac{1}{\eta} \int_0^{h/2} y \Delta H(y) dy \frac{\nabla T}{T}$$
(3)

where  $\beta_{12}$  is the thermo-osmosis coefficient, which characterizes the flow of fluid due to the temperature gradient  $\nabla T$ .  $\eta$  is the viscosity, y is the distance to the surface, y = 0 the position of the first liquid layer, h is the height of the nanochannel, and  $\Delta H$  is the excess of specific enthalpy as compared to the bulk.

The constant bulk viscosity  $\eta$  is used in this work, which has been estimated using the Green–Kubo formula<sup>38</sup>

$$\eta = \frac{V}{k_{\rm b}T} \int_0^t \langle p_{xy}(t) p_{xy}(0) \rangle \mathrm{d}t \tag{4}$$

The simulation details and results can be found in the Supporting Information.

The local specific enthalpy H can be estimated by  $^{28}$ 

$$H(y) = [u_i(y) + p_i^x(y)]\rho(y)$$
 (5)

where  $u_i$  is the energy per particle, including kinetic and potential energy,  $p_i^x$  is the atom-based virial expression for

pressure in the *x*-direction, and  $\rho$  is the local density. The stress tensor for each atom can be estimated<sup>39</sup>

$$p_{ab} = mv_a v_b + \frac{1}{2} \sum_{n=1}^{N} (r_{1a} F_{1b} + r_{2a} F_{2b})$$
(6)

where subscripts of a and b take on values x, y, z to generate components of the tensor,  $r_1$  and  $r_2$  are the positions of the two atoms in the pairwise interaction, and  $F_1$  and  $F_2$  are the forces on the two atoms resulting from the pairwise interaction. The first term is the kinetic energy contribution and the second term is the virial contribution due to intra- and intermolecular interactions. It should be noted that eq 6 may be not accurate for a confined liquid. A more accurate expression has been provided by Todd et al. Here, the reliability of using eq 6 to calculate the enthalpy H has been well verified by Ganti et at. And confirmed further by Fu et al. In addition, Ganti et al. have confirmed that eq 6 provides qualitative results in the diffuse layer and accurate quantitative results out of the diffuse layer. Accordingly, eq 6 is appropriate for the qualitative analysis of the pressure.

Figure 4a shows the excess specific enthalpy as a function of the distance to surface for different liquid-wall interaction energies, and Figure 4b shows the results of  $\beta_{12}$  as a function of liquid-wall interaction energy. For relatively weak liquid-wall interaction energy ( $\varepsilon_{\text{liquid-wall}} < 0.5\varepsilon$ ),  $\Delta H > 0$  leading to a negative  $\beta_{12}$ , and the fluid moves toward the cold side, as shown in outer layers in Figure 3b. The fluid moves out of the

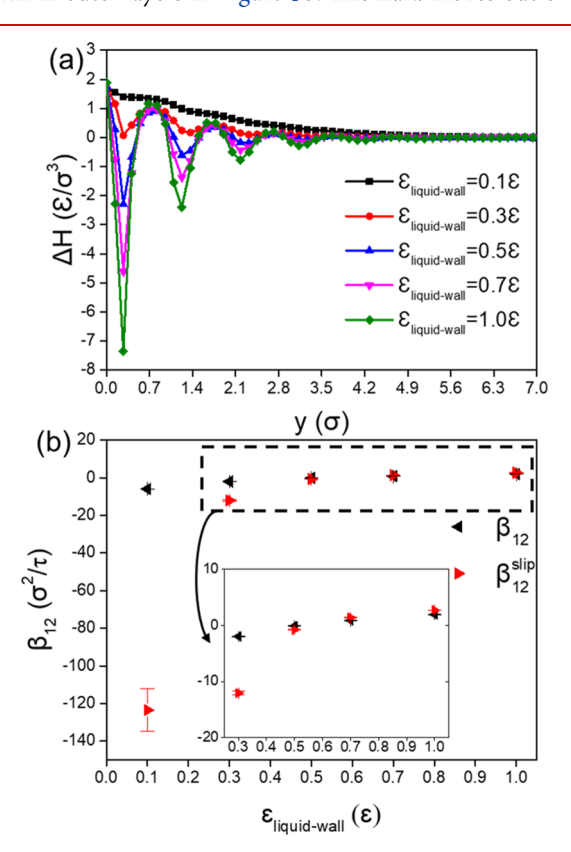


**Figure 4.** (a) Excess specific enthalpy distribution  $\Delta H$  as a function of the distance to the solid surface for different liquid-wall interaction energy  $\varepsilon_{\text{liquid-wall}}$ . (b) Thermo-osmotic coefficient without slip length  $\beta_{12}$  (black labels) and with slip length  $\beta_{12}$  (red labels) as a function of liquid-wall interaction energy. Error bars represent the standard deviation of eight independent simulations.

nanochannel from the outer layers "back to back", which causes a lower pressure inside the nanochannel, as shown in the black circles in Figure 3a. Then the fluid is driven by the caused pressure difference swarming back into the nanochannel from the inner layers, as shown in the inner layers in Figure 3b. Accordingly, multiple convective layers with inverse directions are formed.

When the heated region is in the center, the quantities of thermo-osmotic flows into and backflows out of the left (or right) reservoir are equal. Therefore, no net fluid transport is observed. When the heated region moves leftwards, the caused pressure differences between the inner layers and reservoirs hardly changes, as shown by the pressure distributions in Figure 3. But the pressure gradient in the left inner layer region increases and that in the right decreases, which results in the corresponding enhancement of backflow velocity on the left side and reduction in the right, respectively, as shown in the velocity fields in Figure 3. In particular, the velocity of backflow in the right inner layer decreases to almost zero, Figure 3h. It is expected to be inverted when the heated region moves leftwards further. As a result, a net unidirectional fluid transport emerges. For such fluid transport, different rates can be achieved by tuning the location of the heated region, and the direction can be controlled by moving the heated region leftwards or rightwards.

With the heated region moving left, the temperature gradients in the left side of the heated region become stronger than in the right side, as shown in Figure S9b. Importantly, the net flow is dominated by the pressure gradient difference. The temperature gradients play a minor role in the net flow. Otherwise, the net flow would have been leftward when the heated region moved leftward, consistent with the direction of the larger thermo-osmosis velocity. However, the net flow is rightward.

Using  $\Delta x = 5.4\sigma$ , the effect of liquid-wall interaction energy is studied by tuning  $\varepsilon_{\text{liquid-wall}}$  from  $0.1\varepsilon$  to  $1.0\varepsilon$ . Figure 5a plots the fluid transport as a function of  $\varepsilon_{\text{liquid-wall}}$ . The result reveals two significant features. First, the directions of fluid transport change for strong liquid-wall interaction ( $\varepsilon_{\text{liquid-wall}} > 0.5\varepsilon$ ). Second, the rates are strongly enhanced for relatively weak liquid-wall interaction.

To understand the first feature, the velocity field and pressure distribution for the case of  $\varepsilon_{\text{liquid-wall}}$  = 1.0 $\varepsilon$  are plotted in Figure S8. For  $\varepsilon_{\text{liquid-wall}} = 1.0\varepsilon$ ,  $\Delta H > 0$  leading to a negative  $\beta_{12}$  as shown in Figure 4, and the fluid should move toward hot sides in the outer layers "face to face", as shown in Figure S8b. The fluid moves into the nanochannel from the outer layers. This induces a higher pressure inside the nanochannel, as shown in the black circle in Figure S8a. Then the fluid in the inner layers move out of the nanochannel driven by the induced pressure gradients, as shown in Figure S8b. When the location of the heated region is on the left, the pressure gradient increases in the left inner layer and decreases in the right, which causes the corresponding enhancement of fluid quantity into the left reservoir and reduction into the right reservoir. It finally induces a net fluid transport leftwards and thus, the flow direction changes.

The second feature is assumed to be ascribed to the hydrodynamic slip velocity on the wall surfaces. In fact, the maximum velocity in Figure 3f is about 3 times larger than that in Figure S8b. The amplification of the velocity field should be responsible for the enhanced net fluid transport. However, the values of  $\beta_{12}$  for the above cases, that is,  $\varepsilon_{\text{liquid-wall}} = 0.3\varepsilon$  and

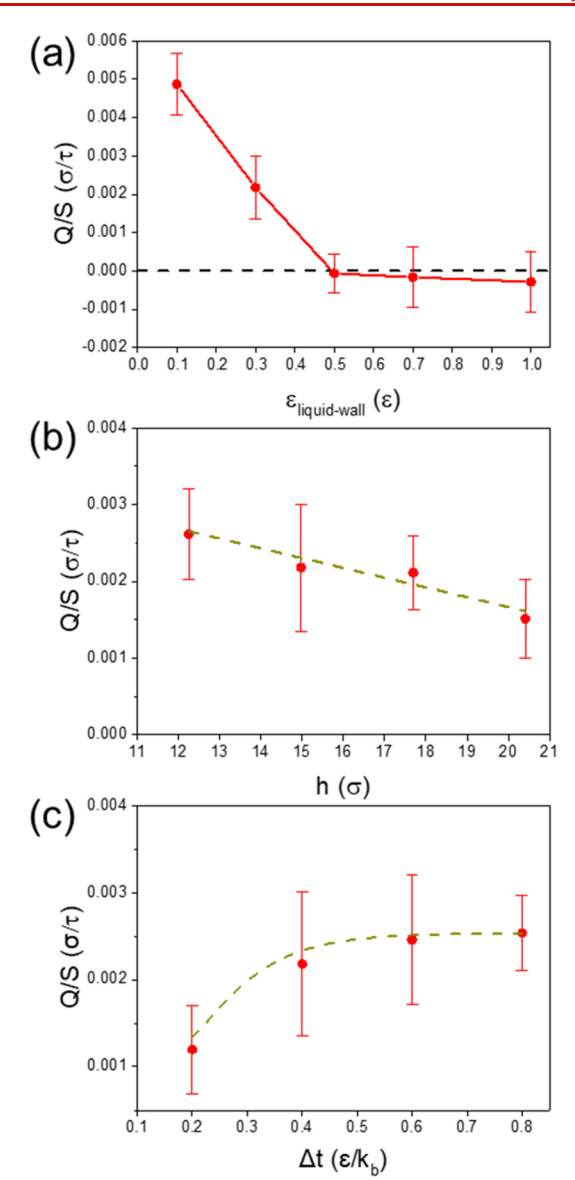


**Figure 5.** (a) Rates of net fluid transport Q/S as functions of liquid-wall interaction energies  $\varepsilon_{\text{liquid-wall}}$  for  $\Delta x = 5.4\sigma$ ,  $\Delta t = 0.4\varepsilon/k_{\text{b}}$ , and  $h = 14.96\sigma$ . Rates of net fluid transport as functions of (b) heights of nanochannels h for  $\Delta t = 0.4\varepsilon/k_{\text{b}}$ , and (c) heating temperature  $\Delta t$  for  $h = 14.96\sigma$ , when  $\varepsilon_{\text{liquid-wall}} = 0.3\varepsilon$  and  $\Delta x = 5.4\sigma$ . The error bars represent the standard deviation of eight independent simulations.

 $1.0\varepsilon$ , are  $-2.0\sigma^2/\tau$  and  $1.9\sigma^2/\tau$ , respectively. They are very close and cannot account for the velocity amplification. Hence, the slip length must be considered. Equation 3 can be rewritten as

$$v_{\rm t} = \beta_{12}^{\rm slip} \frac{\nabla T}{T} = -\frac{1}{\eta} \int_0^{h/2} (y+b) \Delta H(y) \mathrm{d}y \frac{\nabla T}{T} \tag{7}$$

where b is the slip length, and  $\beta_{12}^{\text{slip}}$  is the thermo-osmotic coefficient with the possible effect of slip length. The slip length b can be related to the interfacial friction coefficient  $\lambda^{42}$ 

$$b = \frac{\eta}{\lambda} \tag{8}$$

The friction coefficient  $\lambda$  is related with the equilibrium fluctuations of the friction force in terms of a Green–Kubo relationship<sup>43</sup>

$$\lambda = \frac{1}{Ak_{\rm b}T} \int_0^t \langle F_i(t)F_i(0)\rangle \mathrm{d}t \tag{9}$$

where A is the contact area,  $F_i(t)$  is the total tangential force parallel to the wall surface. We performed another equilibrium MD simulation to estimate the friction coefficient. The simulation details and results can be found in the Supporting Information. The results of corrected  $\beta_{12}^{\rm slip}$  are presented in Figure 4b. The data show that the thermo-osmotic coefficient can be significantly enhanced for the weak liquid-wall interaction energy. Such massive enhancement of the thermo-osmotic slip coefficient due to the hydrodynamic slip velocity has also been reported by Fu et al. <sup>29</sup> The slip velocity has also been found to play a critical role in the performance of diffusio-osmosis, <sup>44</sup> electro-osmosis, <sup>45</sup> and rapid fluid transport through nanomaterials such as carbon nanotubes. <sup>46</sup>

Other than the location of the heated region and surface energy, we also investigate the effect of heating temperature and the height of the nanochannel for the purpose of meeting requirements of practical applications through tuning these parameters. The simulation results are depicted in Figure 5b,c. When the height of the nanochannel is too small, the interfacial layers in the upper and bottom walls may overlap. The situation may become far complex and counterintuitive. 47,48 We do not consider this extremely confined situation. Hence, the minimum of the height is chosen as  $12\sigma$ , larger than twice the thickness of the interfacial layer, to avoid the overlap. It is seen that the fluid transport rates per unit cross area of the nanochannel decrease as the height of the nanochannel increases. The relation between the rate of fluid transport and the temperature difference is almost logarithmic. This dependence is referred to as "log-sensing", 25 which enriches the methods of manipulating fluid in the context of thermoosmosis. We have confirmed that fluid transport also can be achieved with cooling a certain region, which is not reported

Several potential applications of the proposed system can be deduced from the previously mentioned results. One application is for the chip-level cooling. The heat generated by the chips can be employed to produce asymmetric temperature gradients in the channels through proper configurations. The coolant liquids can be circulated without extra pumps. It saves the cost of energy, space, production, and maintenance of the pump machines, well in favor of the trend for miniaturization of electronic devices. Another application is to promote the mixing of matter in cases demanding rapid mixing. In nanofluidics, the flows are laminar due to a very low Reynolds number. The mixing without turbulent eddies depends purely on diffusive processes, which take unacceptably long times. The formed multiple convective layers, as shown in Figure 3b, provide a strategy to enhance the mixing.

In summary, our study has shown novel results for controlled thermo-osmosis flow in localized heated nanochannels. When a particular region is heated near the wall surfaces, multiple convective layers are formed. The flow is driven by thermo-osmosis "back to back" for relatively weak liquid-wall interaction and "face to face" for strong liquid-wall interaction, causing a pressure gradient in the channel by which fluid flows into or out of the nanochannel. Specifically, when the heated region is in the center of the nanochannel, the pressure gradients in the left and right ends are comparable, and no net fluid transport occurs. When the heated region is not in the center, a net fluid transport occurs where fluid is

pumped continuously from one reservoir to another. These results provide guidance for development of future experiments and suggest an alternative approach for manipulation of nanofluidic devices in a precise and noncontact way. Particularly, our finding is promising for chip-level cooling where the heat generated by the chips can be employed to produce asymmetric temperature gradients in the channels through proper configurations. The coolant liquids can thus be circulated without extra pumps.

# ASSOCIATED CONTENT

# **Supporting Information**

The Supporting Information is available free of charge at https://pubs.acs.org/doi/10.1021/acs.nanolett.0c04331.

Supplemental simulations and additional figures; extensive description of the materials including the simulation details, estimation of contact angle, liquid viscosity, friction coefficient and slip length, velocity field and pressure distributions, temperature distributions, and effect of different thermostatting methods (PDF)

### AUTHOR INFORMATION

# **Corresponding Authors**

Dengwei Jing — State Key Laboratory of Multiphase Flow in Power Engineering, Xi'an Jiaotong University, Xi'an 710049, China; Email: dwjing@mail.xjtu.edu.cn

Oleg Prezhdo – Department of Chemistry, University of Southern California, Los Angeles, California 90089, United States; ocid.org/0000-0002-5140-7500; Email: prezhdo@usc.edu

# **Authors**

Xin Wang — State Key Laboratory of Multiphase Flow in Power Engineering, Xi'an Jiaotong University, Xi'an 710049, China

Maochang Liu — State Key Laboratory of Multiphase Flow in Power Engineering, Xi'an Jiaotong University, Xi'an 710049, China; ⊚ orcid.org/0000-0002-2371-4060

Abdulmajeed Mohamad — Schulich School of Engineering, CEERE, The University of Calgary, Calgary, Alberta T2N1N4, Canada

Complete contact information is available at: https://pubs.acs.org/10.1021/acs.nanolett.0c04331

## **Author Contributions**

X.W. and M.L. contributed equally to this work.

#### Notes

The authors declare no competing financial interest.

# ACKNOWLEDGMENTS

The authors gratefully acknowledge the financial support of the National Natural Science Foundation of China (No. 51888103 and 52025061), the financial support from the Royal Society-Newton Advanced Fellowship grant (NAF\R1\191163), and U.S. National Science Foundation (CHE-1900510).

#### REFERENCES

- (1) Bocquet, L.; Charlaix, E. Nanofluidics, from bulk to interfaces. *Chem. Soc. Rev.* **2010**, *39*, 1073–1095.
- (2) Celebi, K.; Buchheim, J.; Wyss, R. M.; Droudian, A.; Gasser, P.; Shorubalko, I.; Kye, J.-I.; Lee, C.; Park, H. G. Ultimate permeation across atomically thin porous graphene. *Science* **2014**, *344*, 289–292.

- (3) O'Hern, S. C.; Boutilier, M. S.; Idrobo, J.-C.; Song, Y.; Kong, J.; Laoui, T.; Atieh, M.; Karnik, R. Selective ionic transport through tunable subnanometer pores in single-layer graphene membranes. *Nano Lett.* **2014**, *14*, 1234–1241.
- (4) Feng, J.; Graf, M.; Liu, K.; Ovchinnikov, D.; Dumcenco, D.; Heiranian, M.; Nandigana, V.; Aluru, N. R.; Kis, A.; Radenovic, A. Single-layer MoS2 nanopores as nanopower generators. *Nature* **2016**, 536, 197–200.
- (5) Secchi, E.; Marbach, S.; Niguès, A.; Stein, D.; Siria, A.; Bocquet, L. Massive radius-dependent flow slippage in carbon nanotubes. *Nature* **2016**, *537*, 210–213.
- (6) Hong, S.; Constans, C.; Surmani Martins, M. V.; Seow, Y. C.; Guevara Carrio, J. A.; Garaj, S. Scalable graphene-based membranes for ionic sieving with ultrahigh charge selectivity. *Nano Lett.* **2017**, *17*, 728–732.
- (7) Tunuguntla, R. H.; Henley, R. Y.; Yao, Y.-C.; Pham, T. A.; Wanunu, M.; Noy, A. Enhanced water permeability and tunable ion selectivity in subnanometer carbon nanotube porins. *Science* **2017**, 357, 792–796.
- (8) Fumagalli, L.; Esfandiar, A.; Fabregas, R.; Hu, S.; Ares, P.; Janardanan, A.; Yang, Q.; Radha, B.; Taniguchi, T.; Watanabe, K.; Gomila, G.; Novoselov, K. S.; Geim, A. K. Anomalously low dielectric constant of confined water. *Science* **2018**, *360*, 1339–1342.
- (9) Lokesh, M.; Youn, S. K.; Park, H. G. Osmotic transport across surface functionalized carbon nanotube membrane. *Nano Lett.* **2018**, 18, 6679–6685.
- (10) Mouterde, T.; Keerthi, A.; Poggioli, A.; Dar, S. A.; Siria, A.; Geim, A. K.; Bocquet, L.; Radha, B. Molecular streaming and its voltage control in ångström-scale channels. *Nature* **2019**, *567*, 87–90.
- (11) Rabinowitz, J.; Cohen, C.; Shepard, K. L. An electrically actuated, carbon nanotube-based biomimetic ion pump. *Nano Lett.* **2020**, *20*, 1148–1153.
- (12) Ostler, D.; Kannam, S. K.; Frascoli, F.; Daivis, P. J.; Todd, B. D. Efficiency of Electropumping in Nanochannels. *Nano Lett.* **2020**, *20*, 3396–3402.
- (13) Van der Heyden, F. H.; Bonthuis, D. J.; Stein, D.; Meyer, C.; Dekker, C. Electrokinetic energy conversion efficiency in nanofluidic channels. *Nano Lett.* **2006**, *6*, 2232–2237.
- (14) Huang, G.; Willems, K.; Bartelds, M.; van Dorpe, P.; Soskine, M.; Maglia, G. Electro-osmotic vortices promote the capture of folded proteins by PlyAB nanopores. *Nano Lett.* **2020**, *20*, 3819–3827.
- (15) Devasenathipathy, S.; Santiago, J. G. Electrokinetic flow diagnostics. In *Microscale Diagnostic Techniques*; Springer: Heidelberg, Berlin, 2005.
- (16) Lippmann, G. Endosmose entre deux liquides de même composition chimique et de températures différentes. *Compt. Rend.* **1907**, *145*, 104–105.
- (17) Yu, L.-H.; Chen, Y.-F. Concentration-dependent thermophoretic accumulation for the detection of DNA using DNA-functionalized nanoparticles. *Anal. Chem.* **2015**, *87*, 2845–2851.
- (18) Wienken, C. J.; Baaske, P.; Rothbauer, U.; Braun, D.; Duhr, S. Protein-binding assays in biological liquids using microscale thermophoresis. *Nat. Commun.* **2010**, *1*, 100.
- (19) Kim, S. J.; Ko, S. H.; Kang, K. H.; Han, J. Direct seawater desalination by ion concentration polarization. *Nat. Nanotechnol.* **2010**, *5*, 297–301.
- (20) Lee, J.; Laoui, T.; Karnik, R. Nanofluidic transport governed by the liquid/vapour interface. *Nat. Nanotechnol.* **2014**, *9*, 317.
- (21) Straub, A. P.; Yip, N. Y.; Lin, S.; Lee, J.; Elimelech, M. Harvesting low-grade heat energy using thermo-osmotic vapour transport through nanoporous membranes. *Nat. Energy.* **2016**, *1* (7), 1–6.
- (22) Keulen, L.; Van Der Ham, L.; Kuipers, N.; Hanemaaijer, J.; Vlugt, T.; Kjelstrup, S. Membrane distillation against a pressure difference. *J. Membr. Sci.* **2017**, *524*, 151–162.
- (23) Kim, S.; Mench, M. Investigation of temperature-driven water transport in polymer electrolyte fuel cell: phase-change-induced flow. *J. Electrochem. Soc.* **2009**, *156*, B353–B362.

- (24) Kim, S.; Mench, M. Investigation of temperature-driven water transport in polymer electrolyte fuel cell: Thermo-osmosis in membranes. *J. Membr. Sci.* **2009**, 328, 113–120.
- (25) Marbach, S.; Bocquet, L. Osmosis, from molecular insights to large-scale applications. *Chem. Soc. Rev.* **2019**, *48*, 3102–3144.
- (26) Barragán, V. M.; Kjelstrup, S. Thermo-osmosis in membrane systems: a review. *J. Non-Equil. Thermody.* **2017**, *42*, 217–236.
- (27) Bregulla, A. P.; Würger, A.; Günther, K.; Mertig, M.; Cichos, F. Thermo-osmotic flow in thin films. *Phys. Rev. Lett.* **2016**, *116*, 188303.
- (28) Ganti, R.; Liu, Y.; Frenkel, D. Molecular simulation of thermosmotic slip. *Phys. Rev. Lett.* **2017**, *119*, No. 038002.
- (29) Fu, L.; Merabia, S.; Joly, L. What controls thermo-osmosis? Molecular simulations show the critical role of interfacial hydrodynamics. *Phys. Rev. Lett.* **2017**, *119*, 214501.
- (30) Ajdari, A. Electro-osmosis on inhomogeneously charged surfaces. *Phys. Rev. Lett.* **1995**, *75*, 755.
- (31) Liu, C.; Li, Z. Molecular dynamics simulation of composite nanochannels as nanopumps driven by symmetric temperature gradients. *Phys. Rev. Lett.* **2010**, *105*, 174501.
- (32) Picallo, C. B.; Gravelle, S.; Joly, L.; Charlaix, E.; Bocquet, L. Nanofluidic osmotic diodes: Theory and molecular dynamics simulations. *Phys. Rev. Lett.* **2013**, *111*, 244501.
- (33) Li, L.; Mo, J.; Li, Z. Nanofluidic diode for simple fluids without moving parts. *Phys. Rev. Lett.* **2015**, *115*, 134503.
- (34) Mo, J.; Li, C.; Li, L.; Wang, J.; Li, Z. Passive nanofluidic diode using non-uniform nanochannels. *Phys. Fluids* **2016**, 28, No. 082005.
- (35) Chikazawa, J. I.; Uwada, T.; Furube, A.; Hashimoto, S. Flow-Induced Transport via Optical Heating of a Single Gold Nanoparticle. *J. Phys. Chem. C* **2019**, *123*, 4512–4522.
- (36) Plimpton, S. Fast parallel algorithms for short-range molecular dynamics. *J. Comput. Phys.* **1995**, *117*, 1–19.
- (37) Derjaguin, B. V.; Churaev, N. V.; Muller, V. M.; Kisin, V. I. Surface forces; Springer: Consultants Bureau, NY, 1987.
- (38) Bushehri, M. K.; Mohebbi, A.; Rafsanjani, H. H. Prediction of thermal conductivity and viscosity of nanofluids by molecular dynamics simulation. *J. Eng. Thermophys.* **2016**, *25*, 389–400.
- (39) Allen, M.; Tildesley, D. Computer simulation of liquids; Oxford: New York, 1989; Vol. 385.
- (40) Todd, B. D.; Evans, D. J.; Daivis, P. J. Pressure tensor for inhomogeneous fluids. *Phys. Rev. E: Stat. Phys., Plasmas, Fluids, Relat. Interdiscip. Top.* **1995**, *52*, 1627.
- (41) Ganti, R.; Liu, Y.; Frenkel, D. Hamiltonian transformation to compute thermo-osmotic forces. *Phys. Rev. Lett.* **2018**, 121, No. 068002.
- (42) Bocquet, L.; Barrat, J.-L. On the Green-Kubo relationship for the liquid-solid friction coefficient. *J. Chem. Phys.* **2013**, *139*, No. 044704.
- (43) Bocquet, L.; Barrat, J.-L. Hydrodynamic boundary conditions, correlation functions, and Kubo relations for confined fluids. *Phys. Rev. E: Stat. Phys., Plasmas, Fluids, Relat. Interdiscip. Top.* **1994**, 49, 3079.
- (44) Ajdari, A.; Bocquet, L. Giant amplification of interfacially driven transport by hydrodynamic slip: Diffusio-osmosis and beyond. *Phys. Rev. Lett.* **2006**, *96*, 186102.
- (45) Joly, L.; Ybert, C.; Trizac, E.; Bocquet, L. Hydrodynamics within the electric double layer on slipping surfaces. *Phys. Rev. Lett.* **2004**, 93, 257805.
- (46) Park, H. G.; Jung, Y. Carbon nanofluidics of rapid water transport for energy applications. *Chem. Soc. Rev.* **2014**, 43, 565–576.
- (47) Fu, L.; Merabia, S.; Joly, L. Understanding fast and robust thermo-osmotic flows through carbon nanotube membranes: Thermodynamics meets hydrodynamics. *J. Phys. Chem. Lett.* **2018**, *9*, 2086–2092.
- (48) Walther, J. H.; Ritos, K.; Cruz-Chu, E. R.; Megaridis, C. M.; Koumoutsakos, P. Barriers to superfast water transport in carbon nanotube membranes. *Nano Lett.* **2013**, *13*, 1910–1914.